Particle Accelerators, 1991, Vol. 36, pp.141–160
Reprints available directly from the publisher
Photocopying permitted by license only

OCTUPOLE CORRECTION OF GEOMETRIC ABERRATIONS FOR HIGH-CURRENT HEAVY-ION BEAMS

D.D.-M. HO
Lawrence Livermore National Laboratory, Livermore, CA 94550
I. HABER
Naval Research Laboratory, Washington D.C. 20375
K. R. CRANDALL
AccSys Technology, Inc., Pleasanton, CA 94566
and
S. T. BRANDON
Lawrence Livermore National Laboratory, Livermore, CA 94550

(Received 20 August 1991, in final form 3 September 1991)

Ignition of an inertially confined thermonuclear pellet by heavy-ion beams requires focusing several beams, each with current in the kiloampere range, onto a focal spot a few millimeters in radius and several meters from the last focusing magnet. Third-order geometric aberrations, caused by nonlinearity in the fringe fields of the quadrupole focusing magnets, increase the focal spot size. Space-charge force further enhances these aberrations through the first-order dynamics primarily because the beam size is increased. These aberrations can be substantial for both full-size and smaller experimental accelerators for heavy-ion fusion. Octupole magnets can substantially reduce these aberrations. A method is described here to determine the octupole locations. The octupole strengths are then minimized using the method of least squares with constraints. Self-consistent particle-in-cell simulations using realistic particle distribution functions verify that the octupoles found from this method effectively suppress the aberrations.

1. INTRODUCTION

Heavy-ion induction linacs are receiving increased attention as drivers in inertial confinement fusion (ICF) [1] for commercial energy production because they can have high repetition rate ($\gg$ 1MHz), [2, 3] high efficiency (up to 40%), [3] and good reliability over many pulses. An important requirement for a heavy-ion driver is the ability to focus high-current beams (in the kiloampere range) onto a millimeter-size spot. However, the third-order geometric aberrations caused by nonlinearity in the fringe fields of the quadrupole magnets in the final focusing system cause significant fraction of beam to fall outside of the desired focal spot radius. This loss of beam can be severe in both full-size and smaller experimental accelerators. Correcting the geometric aberration can therefore be important for accelerators for heavy-ion fusion.

Several authors have investigated the third-order aberrations and the use of octupoles to correct this aberration. Neuffer [4] first pointed out that these aberrations can be severe. Fenster[5] then showed that they can be corrected for low-current beams using octupoles in a point-to-point focusing system (one in which the envelope has zero radius at the starting point and at the focal spot). In addition, Fenster demonstrated a scheme for locating octupoles with low strengths. Based on Fenster's method, Colton[6] calculated the octupole locations and strengths for a low-current focusing system. Maidment and Prior[7] and Hofmann,[8] both using particle-in-cell (PIC) simulations, showed that the third-order aberration in high-current beams can be reduced with the use of octupoles. Maidment and Prior showed that with octupole corrections, about 80% of the beam can fall on the focal spot, but not all the fringe field components have been included in their calculations. Hofmann's study shows that for high-current beams, beam loss is still as high as 50% even with octupole correction.

In this paper, we develop a systematic treatment for effectively suppressing the geometric aberrations for high-current beams using octupoles with relatively low strengths. We demonstrate that space-charge force contributes to third-order aberrations through first-order dynamics. The third-order aberrations are increased by space charge primarily because the beam size is increased. The third-order aberrations can be expressed in terms of the first-order particle trajectory (without aberration), which is calculated using the envelope code TRACE.[10] (TRACE is an interactive, first-order beam dynamics program that calculates the envelopes of a charged-particle beam, including linear space-charge forces, through a user-defined transport system. This code was modified so that it can evaluate the integrals, given in Sections 2 and 3, that describe the particle trajectories under the influence of aberration and octupole fields.) Equating the displacement caused by the third-order aberrations to the displacement caused by the octupoles for test particles at the focal spot, we obtain a system of three coupled equations. In an example presented in this paper, six octupoles are used. Their locations are determined from the condition that causes the diagonal elements of the 3×3 matrix, given by the three coupled equations, to vanish. [This scheme was first proposed by Fenster[5] for point-to-point focusing system. But the focusing systems for high-current beams presented here all have waist-to-waist configuration (i.e., the envelope has zero slope and circular cross section at the starting point and at the focal spot). Thus, the expressions for the aberration and the octupole correction are different here from that of a point-to-point system.] Once the octupole locations are known, their strengths can be further reduced by using the method of least squares with constraints. Calculations also show that the aberrations do not depend sensitively on the exact shape or width of the fringe fields.

The locations and strengths of the octupoles obtained by the method described here are confirmed by two-dimensional (in the transverse directions) PIC simulations using SHIFTXY[11] which include the full self consistent evolution of space charge force. Simulations using realistic particle distribution functions show that the octupoles substantially reduce the aberrations. Unlike most of the previous studies, the lengths of the focusing systems presented here are kept to a minimum. Otherwise, the beam ends tend to expand rapidly due to longitudinal space-charge force[9] for high-current beams. This expansion generates velocity tilts (defined as the relative longitudinal velocity for various parts of the beam with respect to the beam center), which cause chromatic aberrations.

This paper is organized as follows: The expressions for single-particle trajectories to third order are presented and the dominant terms in these expressions are discussed

in Section 2. Section 3 describes the procedure used to determine the locations of the octupoles and the method used to minimize their strengths. Section 4 presents the beamline designs and PIC simulations of a full-size and a smaller experimental final focusing systems. The simulations show that the design procedure for the octupoles is still valid when the full self-consistent evolution of the beam distribution is included. The results are summarized in Section 5. Appendix A presents the derivation of the single-particle equation of motion with space-charge-induced electric field to third order. Appendix B gives a brief description of the method of least squares with constraints which is used to minimize the octupole strengths.

2. PARTICLE TRAJECTORIES TO THIRD ORDER

To obtain particle trajectories to third order, we start from the Lorentz equation

$$\frac{d}{dt}(m\mathbf{v}) = Ze(\mathbf{E} + \mathbf{v} \times \mathbf{B}) \tag{1}$$

Here, e is the electronic unit of charge; Z is the charge state; m is the ion mass; $\mathbf{B}$ is the applied magnetic field; $\mathbf{E}$ is the electric field due to beam space charge; and $\mathbf{v}$ is the particle velocity. The beam is assumed to be long, so the beam longitudinal self electric field can be set to zero.

Define a magnetic scalar potential Φ_m such that the quadrupole magnetic field can be obtained from $\mathbf{B} = -(P/Ze)\nabla\Phi_m$, where $\mathbf{P} = m\mathbf{v}$ is the particle momentum. This potential (which has quadrupole symmetry), can be expressed (to fourth order) as [12]

$$\Phi_m = -xy\ k(z) + \frac{1}{12}(x^2 + y^2)xy\ k''(z) \quad . \tag{2}$$

Here, x and y are the transverse coordinates and z is the direction of beam propagation; $k(z) = (Ze/P)[B(z)/a]$, where $B(z)$ is the magnitude of the pole-tip magnetic field, is assumed to be uniform in the quadrupole interior but decreases at the ends, and the primes represent the derivative of the quantity with respect to z.

We can obtain the single-particle equation of motion to third order by inserting Eq. 2 into Eq. 1, and retaining only the linear part of the space-charge force in the transverse direction. (The higher order space-charge force resulting from beam envelope variation makes a negligible contribution to the aberrations, as shown in Appendix A, and the higher order space-charge force arising from the density profile nonuniformity due to nonzero transverse temperature is also negligible as discussed later in this section.) From this equation, we can derive the equations that describe the particle trajectory in Cartesian corrdinates to third order following the algebric manipulation similar to that in Ref.[13], except that now the total energy of the particle, instead of particle speed, is an invariant. This is true because we now include the beam electrostatic potential which is not included in Ref.[13]. But we still assume that the particle mass is constant since the variation of the particle mass is negligible over the length of the focusing system. When we expand Eq. 1, the terms generated by the electrostatic potential are small and hence we ignore them in the following equations. These equations are

$$x'' + (k - k_{sx})x = f_x^4 \quad , \tag{3a}$$

$$y'' - (k + k_{sy})y = f_y^4 \quad , \tag{3b}$$

where the third-order driving terms from space-charge force and quadrupole fields are

$$\begin{aligned} f_x^4 &= k_{sx}(xx'^2 + xy'^2) - k(\frac{1}{2}xy'^2 - x'yy' + \frac{3}{2}xx'^2) \\ &\quad + k'xyy' + \frac{1}{12}k''(3xy^2 + x^3) \quad , \end{aligned} \tag{4a}$$

$$\begin{aligned} f_y^4 &= k_{sy}(yy'^2 + x'^2y) + k(\frac{1}{2}x'^2y - xx'y' + \frac{3}{2}yy'2) \\ &\quad - k'xyx' - \frac{1}{12}k''(3x^2y + y^3) \quad . \end{aligned} \tag{4b}$$

The space-charge forces per unit mass can be expressed as

$$\begin{aligned} k_{sx}\, x &= \frac{Zem_0\lambda x}{\pi\gamma\varepsilon_0 P^2(r_x + r_y)r_x} \\ k_{sy}\, y &= \frac{Zem_0\lambda y}{\pi\gamma\varepsilon_0 P^2(r_x + r_y)r_y} \quad , \end{aligned}$$

where λ is the line charge density, ε_0 is the permittivity of free space, γ is the relativistic factor, m_0 is the ion rest mass, and r_x and r_y are the semi-axes of the beam with elliptical cross section in the x and y directions, respectively.

The linear space-charge force assumption, which is verified by PIC simulations presented in the following section, is a good one. This is because in the FODO magnetic quadrupole transport channel, the beam is space-charge dominated, and the beam density profile is therefore nearly uniform.[9] As the beam leaves the FODO transport channel and undergoes free expansion before entering the final focusing quadrupoles, the free expansion further reduces any nonuniformity in the density profile.

The homogeneous (first-order) solutions to Eq.3 are

$$x_h = c_x(z)x_0 + s_x(z)x_0' \quad , \tag{5a}$$

$$y_h = c_y(z)y_0 + s_y(z)y_0' \quad , \tag{5b}$$

where c and s are the cosine-like and sine-like solutions and the subscript zero refers to initial conditions. The particular (third-order) solutions to Eq.3, which give the geometric aberration at the focal spot, are

$$x_p = s_x(z_f)\int_0^{z_f} c_x f_x^4\, dz - c_x(z_f)\int_0^{z_f} s_x f_x^4\, dz \quad , \tag{6a}$$

$$y_p = s_y(z_f)\int_0^{z_f} c_y f_y^4\, dz - c_y(z_f)\int_0^{z_f} s_y f_y^4\, dz \quad , \tag{6b}$$

where z_f is the longitudinal distance from the starting point of the integration to the focal spot.

Inspection of Eq.4 shows that f_x^4 and f_y^4 are large for large x and y. Thus, in calculating the aberration, we only calculate the trajectories of those particles that spend most of their time near the edge of the beam envelope. Numerical calculations based on the examples in Section using TRACE show that particles at the edge of the beam envelope, but with $x_0' = y_0' = 0$ just before the beam undergoes free-space expansion, remain close to the beam edge all the way to the focal spot. In contrast, particles originally located at the beam center, but with the maximum x_0' and y_0' allowed by the beam phase space ellipse, do not get to the beam edge. This is because (for the examples used here) the beam space-charge force is substantially greater than the gradient of the thermal pressure. Thus, we only calculate thetrajectories for the particles at beam edge but with $x_0' = y_0' = 0$ for the purpose of obtaining the locations and strengths of the octupoles.

The third-order driving terms (f_x^4 and f_y^4) in Eq.6 are then expressed in terms of the homogeneous solution (with $x_0' = y_0' = 0$). After some integration by parts to remove the k'' terms, we can express Eq.6 to third-order accuracy as

$$\begin{aligned} x_p^4 &= s_x(z_f)\int_0^{z_f}\Big[x_0y_0^2(k_{sx}c_x^2c_y'^2-\frac{1}{2}kc_x^2c_y'^2+kc_xc_x'c_yc_y'+\frac{1}{2}k'c_x^2c_yc_y' \\ &\quad -\frac{1}{2}k'c_xc_x'c_y^2)+x_0^3(k_{sx}c_x^2c_x'^2-\frac{3}{2}kc_x^2c_x'^2-\frac{1}{3}k'c_x^3c_x')\Big]\,dz \\ &\quad -c_x(z_f)\int_0^{z_f}\Big[x_0y_0^2(k_{sx}s_xc_xc_y'^2-\frac{1}{2}ks_xc_xc_y'^2+ks_xc_x'c_yc_y' \\ &\quad +\frac{1}{2}k's_xc_xc_yc_y'-\frac{1}{4}k's_x'c_xc_y^2-\frac{1}{4}k's_xc_x'c_y^2)+x_0^3(k_{sx}c_x^2c_x'^2 \\ &\quad -\frac{3}{2}ks_xc_xc_x'^2-\frac{1}{4}k'c_x^2s_xc_x'-\frac{1}{12}k'c_x^3s_x')\Big]\,dz \quad , \end{aligned} \tag{7a}$$

$$\begin{aligned} y_p^4 &= s_y(z_f)\int_0^{z_f}\Big[x_0^2y_0(k_{sy}c_x'^2c_y^2+\frac{1}{2}kc_x'^2c_y^2-kc_xc_x'c_yc_y'+\frac{1}{2}k'c_x^2c_yc_y' \\ &\quad -\frac{1}{2}k'c_xc_x'c_y^2)+y_0^3(k_{sy}c_y^2c_y'^2+\frac{3}{2}kc_y^2c_y'^2+\frac{1}{3}k'c_y^3c_y')\Big]\,dz \\ &\quad -c_y(z_f)\int_0^{z_f}\Big[x_0^2y_0(k_{sy}c_x'^2s_yc_y+\frac{1}{2}kc_x'^2s_yc_y-kc_xc_x's_yc_y' \\ &\quad -\frac{1}{2}k'c_xc_x's_yc_y+\frac{1}{4}k'c_x^2s_y'c_y+\frac{1}{4}k'c_x^2s_yc_y')+y_0^3(k_{sy}c_y^2c_y'^2 \\ &\quad +\frac{3}{2}ks_yc_yc_y'^2+\frac{1}{4}k'c_y^2s_yc_y'+\frac{1}{12}k'c_y^3s_y')\Big]\,dz \quad . \end{aligned} \tag{7b}$$

The assumption of a flat density profile near the focal spot can break down for non K-V distributions. But this does not introduce noticeable error when one uses Eq.7 for two reasons. First, the breakdown occurs near the focus, so that the contribution of the nonlinear electric field to the integrals (which is over the entire focusing system) in Eq.7 is small. Second, the integrated effect of the space-charge electric field on particle trajectories is less than the integrated effect of magnetic focusing forces.

Numerical calculations using TRACE for the focusing systems given in Section 4 show that Eq. 7 which is valid to third order, is a good approximation to Eq. 6, i.e., the discrepancy is within 3%. These calculations also show that terms not proportional to k' contribute only a few percent to the integrals in Eq.7 and thus the terms proportional to k, k_{sx}, and k_{sy} can be ignored. (In particular, terms proportional to k_{sx} and k_{sy} contribute only about 1% to the integral, according to calculations for the examples given in Section 4.) Also, $c_x(z_f)x_0$ and $c_y(z_f)y_0$ are small (i.e., about 1.5%) compared with $s_x(s_f)x_0$, and $s_y(z_f)y_0$, respectively, and can therefore be ignored. Consequently, Eq. 7 can be approximated by

$$x_p^4 \cong s_x(z_f)\int_0^{z_f}\left[x_0y_0^2(\frac{1}{2}k'c_x^2c_yc_y' - \frac{1}{2}k'c_xc_x'c_y^2) - x_0^3(\frac{1}{3}k'c_x^3c_x')\right]dz \quad , \tag{8a}$$

$$y_p^4 \cong s_y(z_f)\int_0^{z_f}\left[x_0^2y_0(\frac{1}{2}k'c_x^2c_yc_y' - \frac{1}{2}k'c_xc_x'c_y^2) + y_0^3(\frac{1}{3}k'c_y^3c_y')\right]dz \quad . \tag{8b}$$

Thus, in calculating the third-order aberrations in the final focusing systems for high-current beams, the space-charge contribution enters only in obtaining the first-order solution but does not appear explicitly in the approximate expressions for the third-order aberrations.

The above expressions show that the aberrations are important when either the beam envelope is large or the beam momentum is small (since k is inversely proportional to momentum). Equation 8 is now in a convenient form for calculating the octupole correction. The scheme for obtaining the locations and strengths of the octupoles is described in the following section.

3. OCTUPOLE CORRECTION OF GEOMETRIC ABERRATION

The method to determine the octupole locations and strenghts is described in this section. To determine the octupole locations for a waist-to-waist focusing system, we first obtain a system of three coupled equaxtions that equate the displacement caused by the aberrations to the displacement caused by the octupoles for test particles at the focal spot. The driving terms resulting from octupole fields for the single-particle equation of motion are [12]

$$f_x^8 = \frac{Ze}{P}\frac{B_8}{a^3}x(3y^2 - x^2) \quad , \tag{9a}$$

$$f_y^8 = \frac{Ze}{P}\frac{B_8}{a^3}y(3x^2 - y^2) \quad , \tag{9b}$$

where a and B_8 are the octupole bore radius and pole-tip magnetic field, respectively.

If we assume that the octupoles are thin (i.e., transverse particle excursion is negligible when the particle is traversing an octupole), then by Eq. 6 the octupole contribution to the particle displacement at the focal spot can be approximated by

$$\begin{aligned} x_p^8(z_f) &= \frac{Ze}{P}s_x(z_f)\sum_i \frac{B_{8i}\ell_i}{a_i^3}\left[3c_x^2(z_i)c_y^2(z_i)x_0y_0^2 - c_x^4(z_i)x_0^3\right] \\ &\quad -\frac{Ze}{P}c_x(z_f)\sum_i \frac{B_{8i}\ell_i}{a_i^3}\left[3s_x(z_i)c_x(z_i)c_y^2(z_i)x_0y_0^2 - s_x(z_i)c_x^3(z_i)x_0^3\right] \quad , \end{aligned} \tag{10a}$$

$$\begin{aligned} y_p^8(z_f) &= \frac{Ze}{P}s_y(z_f)\sum_i \frac{B_{8i}\ell_i}{a_i^3}\left[3c_x^2(z_i)c_y^2(z_i)x_0^2y_0 - c_y^4(z_i)y_0^3\right] \\ &\quad -\frac{Ze}{P}c_y(z_f)\sum_i \frac{B_{8i}\ell_i}{a_i^3}\left[3s_y(z_i)c_x^2(z_i)c_y(z_i)x_0^2y_0 - s_y(z_i)c_y^3(z_i)y_0^3\right] \quad , \end{aligned} \tag{10b}$$

where ℓ_i and z_i are the length and location of the ith octupole. The quantity $B_{8i}\ell_i$ is called the strength s_i of the ith octupole. Again $c_x(z_f)x_0$ and $c_y(z_f)y_0$ were found to be small (i.e., about 5%) compared with $s_x(z_f)x_0'$ and $s_y(z_f)y_0'$, respectively and thus terms proportional to $c_x(z_f)$ and $c_y(z_f)$ can be omitted.

Equations 8 and 10 indicate that a minimum of three octupoles suffices to essentially cancel the third-order aberrations if

$$\begin{aligned} \frac{Ze}{P}\sum_{i=1}^{3} c_x^4(z_i)\frac{s_i}{a_i^3} &= h_x \quad , \\ \frac{Ze}{P}\sum_{i=1}^{3} 3c_x^2(z_i)c_y^2(z_i)\frac{s_i}{a_i^3} &= h_{xy} \quad , \\ \frac{Ze}{P}\sum_{i=1}^{3} c_y^4(z_i)\frac{s_i}{a_i^3} &= h_y \quad , \end{aligned} \tag{11}$$

where

$$
\begin{aligned}
h_x &= -\int_0^{z_f} \frac{1}{3} k' c_x^3 c_x' dz \quad , \\
h_{xy} &= -\int_0^{z_f} (\frac{1}{2} k' c_x^2 c_y c_y' - \frac{1}{2} k' c_x c_x' c_y^2) dz \quad , \\
h_y &= \int_0^{z_f} \frac{1}{3} k' c_y^3 c_y' dz \quad .
\end{aligned}
$$

Since Eq. 11 is independent of particle initial positions, it is valid for any particle without transverse motion at the waist. Equation 11 is also a good approximation for all the particles, except those at the tail of the velocity distribution, when the transverse thermal motions is included. This is because (for the examples studied here) thermal motion is small compared with the motion induced by magnetic and space-charge forces. The values of h_x, h_{xy}, and h_y are obtained by numerical integration using TRACE. Thus, the strengths of the octupoles are uniquely determined by the matrix equation, Eq. 11, if the octupole locations are known. (Knowing the locations also gives a_i because a_i is determined by the envelope size.)

The locations of the octupoles are chosen so that the coefficients of the above matrix equation are maximized. This, in principle, can give octupoles with low strengths. However, if we use just three octupoles, their strengths are still unacceptably high for the examples used in this paper. This is because all the coefficients of s_i are positive, while signs on the right-hand side of the equations change. Thus the effects of some of the octupoles are cancelled by those of others.

We find that the octupole strengths can be much lower if we use six octupoles arranged as three pairs of octupoles. The two elements in each pair have equal but opposite strengths, so that these octupoles can be arranged in such a way that the diagonal elements of the matrix (the left-hand-side of Eq.11) are zero. The vanishing of the diagonal weakens the cancellation of the effects of some octupoles by those of others. This means that the first, second, and third octupole pairs have no effect on the h_x, h_{xy}, and h_y aberration terms, respectively. Equation 11 now becomes

$$
\begin{aligned}
\frac{Ze}{P} \sum_{i=1}^{3} \left[c_x^4(z_i) - c_x^4(z_i^*) \right] \frac{s_i}{a_i^3} &= h_x \quad , \\
\frac{Ze}{P} \sum_{i=1}^{3} 3 \left[c_x^2(z_i) c_y^2(z_i) - c_x^2(z_i^*) c_y^2(z_i^*) \right] \frac{s_i}{a_i^3} &= h_{xy} \quad , \\
\frac{Ze}{P} \sum_{i=1}^{3} \left[c_y^4(z_i) - c_y^4(z_i^*) \right] \frac{s_i}{a_i^3} &= h_y \quad ,
\end{aligned}
\tag{12}
$$

where z_i^* refers to the location of the octupole whose strength is equal but opposite to the octupole at z_i.

To determine the locations of the six octupoles, we use TRACE to determine the values of $c_x^4, c_x^2 c_y^2$ and c_y^4 vs z for a given final-focusing beamline design. Then the octupole locations are determined so that the diagonal elements of the above matrix (the left-hand-side of Eq.12) vanish, whereas the other coefficients in the matrix are as large

as possible. In principle, the octupole strengths are now determined. However, if we further let the octupole strengths be independent of each other, with the octupoles remain at the same location, the octupole strengths can be further reduced by using the method of least squares with constraints (see Appendix B). This method is valid because if the octupoles are at other locations, their strengths are usually higher even after the method of least squares with constraints is applied. In the following section, PIC simulations verify that the octupoles determined by the scheme described here substantially increase the fraction of beam hitting the spot.

The scheme described here uses thin idealized octupoles. But this can be modified easily to include the fact that the octupoles have nonzero length, so that the magnetic field B_8 in Eq.9 falls off at the ends. First, we treat the octupoles as delta functions and obtain their locations and strengths. The delta function octupoles are then replaced with octupoles of nonzero length centered at these locations. From the strengths of the delta-function octupoles, we can then estimate the lengths of these octupoles. Knowing the lengths should allow one to determine the shape of B_8 as a function of z. We then replace f_x^4 and f_y^4 in Eq. 6 by f_x^8 and f_y^8 given by Eq. 9. After performing the numerical integrations in Eq. 6, we recover a matrix equation similar to Eq. 11. Because we now have the coefficients for the matrix, the strengths of the octupoles can be readily obtained.

4. NUMERICAL EXAMPLES AND PIC SIMULATIONS

Two final focusing systems, with 5-kA and 8-mA beam current, have been designed using TRACE. We first present the result from the 5-kA design. Figure 1 shows the final focusing system for the 5-kA, 10-GeV beam with atomic mass 210, unnormalized emittance 20 mm·mrad, and Z = 2. We chose a 10-GeV beam with Z = 2 because a present design for a typical heavy-ion driver [3] has energy between 5 and 15 GeV and Z of 1 to 3. The beam is shown going through the last two periods of a magnetic quadrupole transport channel. This is followed by four magnets that change the beam into a waist with circular cross section having a 3.46-cm radius. The beam then undergoes radial expansion due to space-charge force and is finally focused by four large aperture quadrupoles onto a focal spot with 3-mm radius. (It is important to note that the focusing characteristics appear to depend on the configuration of the inital waist. For example, a configuration with asymmetric waists having a small minor radius, e.g., about 1 cm, was found to exhibit strong sensitivity to the initial beam distribution. Substantial spot degradation is occured (e.g., 20% of beam particles fall outside the desired 3-mm focal spot results) when the initial particle distribution at the waist was other than Kapchinskij-Vladimirskij (K-V), e.g., semi-Gaussian (uniform in density and Gaussian in velocity).[14] Each of the final focusing quadrupoles is assumed to have fringe fields that fall off linearly at the ends over a 0.5 m taper centered around the nominal magnet end. The magnetic field gradients of the magnets are given in Table 1. In designing the beamline, we have minimized the distance between the entrance of the first final-focusing quadrupole and the exit of the last final-focusing quadrupole. This was done to minimize the development of longitudinal velocity tilts at the beam ends arising from electrostatic repulsion along the beam.[9]

To obtain the locations and strengths of the octupoles, we first calculate the integrals in Eq.12 using TRACE. The starting point of the numerical integration is at the waist

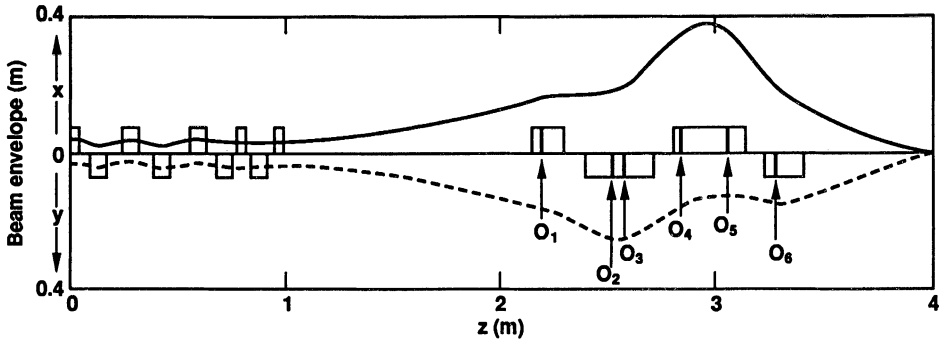

FIGURE 1 Final focusing system for charge-state-2, 5-kA, 10-GeV beam with atomic mass 210 and normalized emittance 20 mm·mrad. The upper and lower curves show the envelope in the x- and y-directions, respectively. $O_1 - O_6$ label the centers of the six octupoles.

prior to the beam expansion. Using the procedures described in Section 3, we obtain the locations and strengths of the octupoles. Then, their strengths, which are listed in Table 1, are obtained using the method of least squares with constraints. The values in the table assume an octupole pole-tip radius of 0.4 m. In reality, however, some of the octupoles can have radii less than 0.4 m in this system, and hence their strengths can be reduced. The maximum excursions of the envelopes in the x and y direction are found to approach each other as the length of the focusing system increases. This should reduce the maximum octupole strength. However, increasing the system length increases chromatic aberration caused by longitudinal velocity tilts. Thus the system must generally be optimized with these considerations in mind.

Because the scheme described for calculating aberrations and their correction assumes zero transverse particle motion at the waist and relies on the linearity of the transverse beam electric field, there is no provision for including the effects of the self-consistent evolution of the beam distribution function. It was therefore necessary to confirm the validity of this scheme by performing self consistent PIC simulations. In the simulation using SHIFTXY code, automatic rezoning of the mesh as the beam expands was used to minimize truncation errors in the numerical solution for the electric field. Using a 2.5-cm longitudinal step and a 256 $\times$ 256 mesh in simulations with an initial K-V distribution, rms radius were generally found to agree to within 1% of the envelope solution up to the spot. Up to 64,000 particles were used to facilitate smooth diagnostics.

If the geometric aberrations are absent, almost 100% of the beam falls onto the 3-mm spot for a K-V distribution, but the fraction of the beam hitting the spot falls to about 50% when aberration is included, as shown in Fig. 2. This figure also shows that the fraction increases to about 95% with octupole corrections. The phase-space projections at the focal spot are shown in Fig.3. In this figure, the projection on the x–y configuration space shows that the aberration is concentrated along the x–axis. This is because the maximum transverse excursion of the beam envelope is larger in the x direction than in they direction. For a semi-Gaussian distribution, Fig. 4 shows that almost 95% of the beam falls onto the spot without aberration, but this figure drops to below 50% with aberration. With octupole correction, the fraction increases to about 90%. The phase-space projections at the focal spot are shown in Fig. 5. The fact that the fraction of the beam on the spot is about the same for both K-V and semi-Gaussian distributions

TABLE 1 System parameters for charge-state-2, 5-kA, 10-GeV beam with atomic mass 210 and unnormalized emittance 20 mm·mrad.

- Magnetic field gradients, lengths of the quadrupoles, and distance between the quadrupoles in the FODO transport system are ± 100.0 T/M, 0.75 m, and 0.75 m, respectively.
- Single-particle phase advance (degree per focusing period) with and without space charge are 3.4 and 51.3, respectively.
- Parameters of the last four quadrupoles before the beam undergoes free-space expansion:

Quadrupole number	Magnetic field gradient (T/m)	Quadrupole length(m)	Distance of quadrupole center to the waist (m)
Q_1	−19.41	0.825	−2.9625
Q_2	18.53	0.450	−2.1500
Q_3	−96.23	0.825	−1.3375
Q_4	114.12	0.475	−0.4125

- Length of free-expansion region is 11.45 m
- Parameters of the final focusing quadrupoles:

Quadrupole number	Magnetic field gradient (T/m)	Quadrupole length(m)	Distance of quadrupole center to the waist (m)
Q_5	7.80	1.475	12.1875
Q_6	−11.08	3.250	15.4750
Q_7	13.72	3.250	19.6000
Q_8	−17.74	1.775	23.1125

- Parameters of the octupoles (assume 0.4 m pole-tip radius):

Octupole number	Strength Bℓ (T·m)	Distance of the octupole center to the waist (m)
O_1	0.18	11.8592
O_2	−0.32	15.0964
O_3	0.02	15.6544
O_4	0.55	18.2849
O_5	−0.69	20.4570
O_6	0.84	22.7141

- Distance between the last focusing quadrupole and the focal spot is 6.0 m.

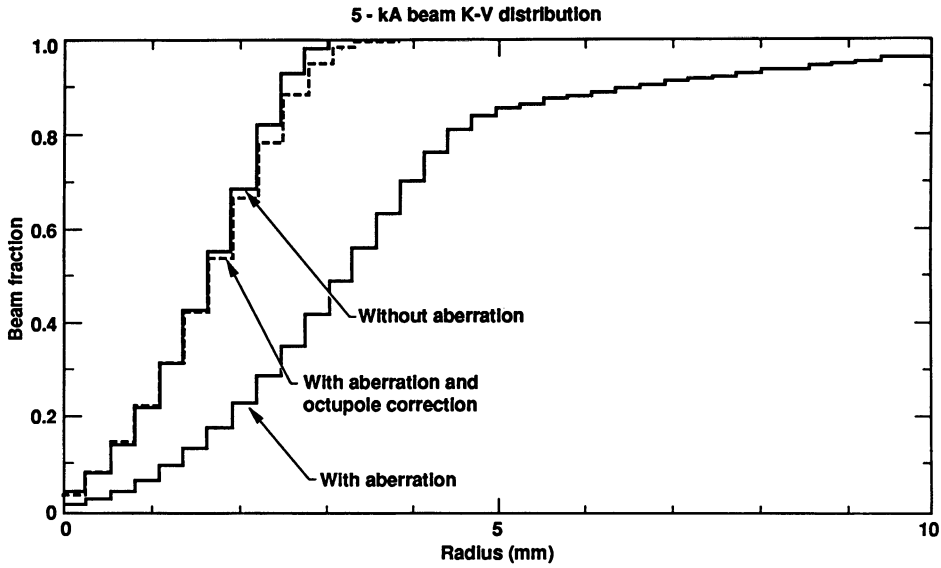

FIGURE 2 Beam fraction vs distance from the center of the focal spot for a 5-kA beam with initial K-V distribution.

indicates that the effect of higher-order electric field induced by the nonuniform density profile caused by the nonzero transverse temperature is small.

In these PIC simulations we started the simulation at the beam waist. We have also performed simulations which started at several FODO periods (up to four) upstream. Comparison of these simulations indicates that the fraction of beam on the spot is essentially independent of where we start the simulation. These simulations also show that the nonlinear magnetic field increases the emittance by a fractor of about two to three in the x direction at the spot but the octupoles restore the emittance back to approximately the original value.

We have sampled the fraction of beam inside a 3-mm radius at various locations near the focal spot and no substantial increase in the fraction has been observed. We have also attempted to adjust the quadrupole strengths so that particles started at a given radius at the waist fall on the same location at the focal spot as if the aberration were absent. However, PIC simulations show that the improvement of the fraction of beam on spot is small, e.g., from 50% to about 60%. Furthermore, any adjustment in the quadrupole strengths to minimize the aberrations only works for that value of current. Using octupoles, on the other hand, will correct over a range of current if the beam particle density is preserved.

The second case is the final focusing system for a smaller-scale experiment with an 8-mA beam which can also be subject to significant geometric aberrations. The hardware for this focusing experiment will be constructed at the Lawrence Berkeley Laboratory.[15] The beam's energy is 0.12 MeV, atomic mass is 132, $Z = 1$, and unnormalized emittance is 62.5 mm·mrad. The beam waist has a radius 14 mm before the free-space expansion

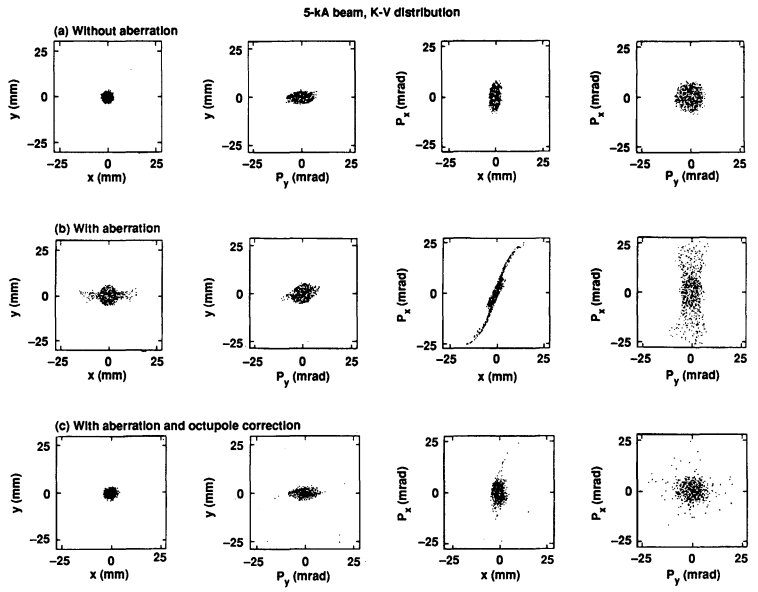

FIGURE 3 Phase space projections at the focal spot for a 5 kA beam with initial K-V distribution. (a) Without aberration; (b) with aberration; (c) with aberration and octupole correction.

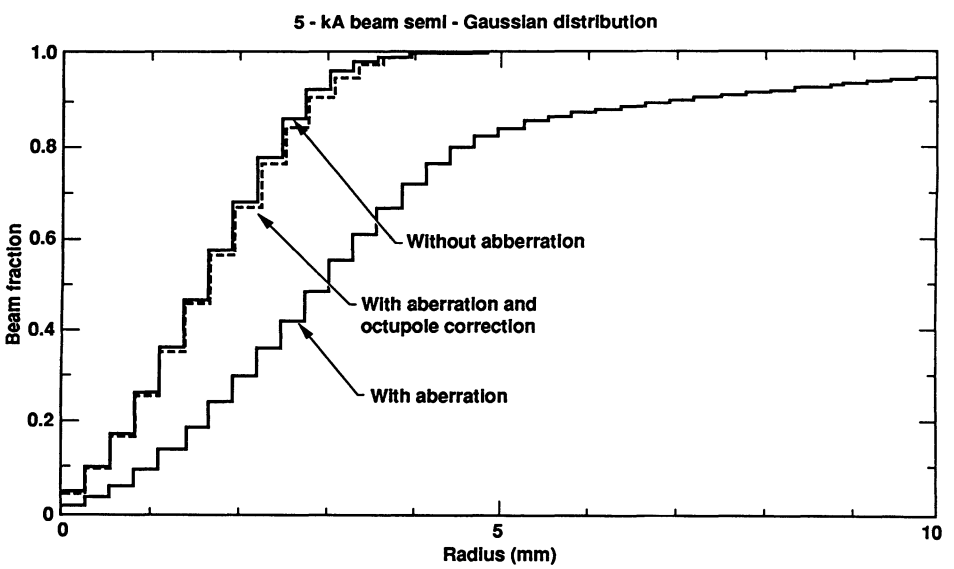

FIGURE 4 Beam fraction vs distance from the center of the focal spot for a 5 kA beam with initial semi-Gaussian distribution.

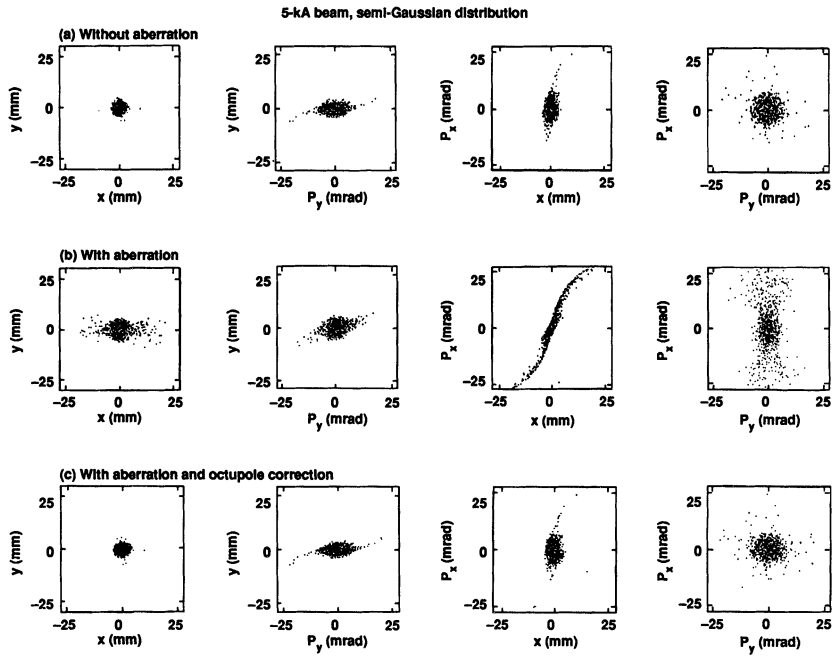

FIGURE 5 Phase-space projections at the focal spot for a 5-kA beam with initial semi-Gaussian distribution. (a) Without aberration; (b) with aberration; (c) with aberration and octupole correction.

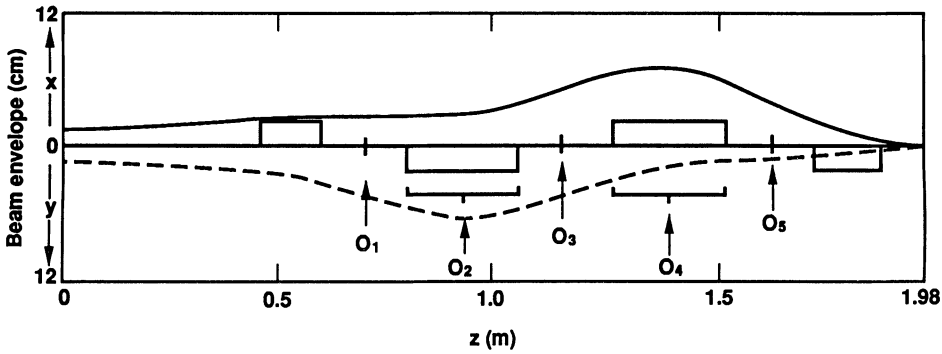

FIGURE 6 Final focusing system for charge-state-1, 8 mA, 0.12 MeV beam with atomic mass 132 and unnormalized emittance 62.5 mm·mrad. The solid line shows the envelope in the x-direction and the dotted line shows the envelope in the y-direction. The upper and lower curves show the envelope in the x- and y-directions, respectively. $O_1 - O_5$ label the locations of the five octupoles.

begins. The focal spot size is 2.5 mm. The configuration of this system is shown in Fig. 6. Although the transverse dimensions of the beam envelope for this case are much smaller than that for the 5-kA case, the geometric aberrations are still large because the beam energy is low.

We did not follow the scheme described above for obtaining the octupole locations. Instead, we choose the most convenient locations, from the engineering point of view, for these octupoles. We put an octupole between each pair of the final focusing quadrupoles and put a octupole inside the second and third quadrupoles. The octupoles inside the quadrupoles have the same length as the quadrupoles. The octupole strengths are then obtained using the method of least squares with constraints. Calculations show that for semi-Gaussian distributions, the fraction of beam on spot is about 88% and 52% without and with aberrations, respectively. The fraction increases to about 80% with octupole correction. The quadrupole and octupole strengths are given in Table 2.

The calculations presented here are carried only to third order in the equations of motion because contribution to geometric aberrations from higher-order terms is small. For example, the magnitude of the sixth-order term in the quadrupole expansion of the magnetic scalar potential Φ_m (Eq. 2) is $(1/384)(Ze/P)(x^2+y^2)xy[B^{iv}(z)/a]$, which is small compared with the fourth-order term (which gives the Lorentz force to third order). Similarly, the sixth-order octupole scalar potential is $(1/20)(Ze/P)(x^3y - xy^3)(x^2 + y^2)(B_8''(z)/a^3)$, which is again small compared with the lowest-order term.

5. CONCLUSION

Third-order geometric aberrations, caused by nonlinearity in the fringe fields of the quadrupole focusing magnets, can be severe in the final focusing systems for both full-size and smaller experimental accelerators. A scheme has been presented for obtaining the locations and strengths of octupoles to correct these aberrations for high-current beams. By recognizing that the space-charge effect does not contribute significantly to the third-order trajectories, one can conveniently obtain the locations of the octupoles by

TABLE 2 System parameters for charge-state-1, 8-mA, 0.12-MeV, beam with atomic mass 132 and unnormalized emittance 62.5 mm·mrad.

- Parameters of the final focusing quadrupoles:

Quadrupole number	Magnetic field gradient(T/m)	Quadrupole length (m)	Distance of quadrupole center to the waist (m)
Q_1	8.696	0.15	0.555
Q_2	−9.359	0.25	0.950
Q_3	10.650	0.25	1.405
Q_4	−22.310	0.15	1.805

- Parameters of the octupoles (assume 0.1 m pole-tip radius):

Octupole number	Pole-tip magnetic field (T)	Octupole length (m)
O_1	0.125	0.10
O_2	−0.089	0.25
O_3	0.407	0.10
O_4	−0.101	0.25
O_5	−0.014	0.10

- Distance between the last focusing quadrupole and the focal spot is 0.15 m.

solving a system of three coupled linear equations, and then their strengths are minimized by the method of least squares with constraints. Particle-in-cell simulations confirm that the octupoles found using this prescription are effective in suppressing the geometric aberrations for high-current beams.

ACKNOWLEDGEMENTS

We thank E. P. Lee, R. O. Bangerter, E. Colton, S. Fenster, R. D. Ryne, and H. Wollnik for discussions. We are grateful to P. W. Murphy for editing the manuscript. Work performed under the auspices of the U.S. Department of Energy by the Lawrence Livermore National Laboratory under contract number W-7405-ENG-48, by AccSys Technology under SBIR contract number DE-AC03-89ER80768, and under the auspices of the director, Office of Energy Research, U.S. Department of Energy under contract number DE-AC03-76SF00098, Office of Basic Energy Sciences, Advanced Energy Project Division, through memorandum request number 4566410 from the Lawrence Berkeley Laboratory.

REFERENCES

1. R. O. Bangerter and D. Keefe, *Nucl. Fusion* **26**, 1741 (1986).
2. D. J. Dudjiak and W. B. Hermannsfeldt, Heavy Ion Inertial Fusion, *Am. Inst. of Phys. Conf. Proc.* **152**, M. Reiser, T. Godlove, and R. O. Bangerter, Eds., Washington, D.C. (1986), p. 111.
3. J. Hovingh, V. O. Brady, A. Faltens, D. Keefe, and E. P. Lee, Fusion Technology **13**, 255 (1988).
4. D. Neuffer, Lawrence Berkeley Laboratory, Berkeley, Calif., LBL HIF Note HI-FAN-36 (1978).
5. S. Fenster, *Proceedings of the Heavy Ion Fusion Workshop*, W. B. Hermannsfeldt, Ed., Lawrence Berkeley Laboratory Report LBL-10301 (1980), p.355.
6. E. Colton, *Proceedings of the Heavy Ion Fusion Workshop*, W. B. Hermannsfeldt, Ed., Lawrence Berkeley Laboratory Report LBL-10301 (1980), p. 365.
7. J. B. M. Maidment and C. R. Prior, *Proceedings of the Symposium on Accelerator Aspects of Heavy Ion Fusion*, Gesellschaft für Schwerionenforschung, Report GSI-82-8 (1982), p. 376.
8. I. Hofmann, I. Bozsik, and S. Sudo, presentation at Univ. of Wisconsin (1980).
9. D. D.-M. Ho, S. T. Brandon, and E. P. Lee, 'Longitudinal Beam Compression for Heavy-Ion Inertial Fusion,' *Part. Accelerators*, **35**, 15(1991).
10. K. R. Crandall, Los Alamos National Laboratory, Los Alamos, N. Mex., Report LA-11054-MS (1987).
11. I. Haber and H. Rudd, 'Linear Accelerator and Beam Optics Codes', *Am. Inst. of Phys. Conf. Proc.* **177**, New York (1988), p. 161; I. Haber, 'High Current, High Brightness, and High Duty Factor Ion Injectors', *Am. Inst. of Phys. Conf. Proc.* **177**, New York (1986), p. 107.
12. P. F. Mead, Jr., Ph.D. thesis, University of California and Lawrence Berkeley Laboratory, University of California, Report UCRL-10807 (1963).
13. K. G. Steffen, *High Energy Beam Optics*, Ch. 1 (Interscience Publishers, John Wiley and Sons, New York, 1965).
14. D. D.-M. Ho, K. R. Crandall, and I. Haber, paper forthcoming.
15. K. R. Crandall and D. D.-M. Ho, 'Scaling Experiment for Heavy-Ion Fusion Final Focusing,' *Part. Accelerators* (in press).

APPENDIX A: DERIVATION OF THE SINGLE-PARTICLE EQUATIONS OF MOTION WITH SPACE-CHARGE-INDUCED ELECTRIC FIELD TO THIRD ORDER

In this appendix, we derive the single-particle equations of motion, with space-charge electric field, to third order during the beam expansion in the section between the FODO latice and the final focusing quadrupoles; see Fig. 1. The third-order electric field terms arise from the fact that the beam envelope is varying. Since the waist is circular prior to the expansion, the beam is axisymmetric, with radius $a(z)$, in the expansion section. The beam is assumed to be surrounded by a perfectly conducting cylinder of radius b. We first demonstrate that the geometric aberrations induced by the space-charge electric field are small and then argue that this is also the case for the rest of the final focusing system.

To obtain the higher-order electric fields for the equation of motion, Eq. 1, we start with Faraday's and Gauss's laws:

$$\nabla \times \mathbf{E} = -\frac{\partial \mathbf{B}}{\partial t} \quad , \tag{A.1}$$

$$\nabla \cdot \mathbf{E} = \frac{\rho(z)}{\varepsilon_0} \quad , \tag{A.2}$$

where $\rho(z)$ is the charge density. We assume that the beam is infinitely long with constant current (or line charge density) and energy. Hence $\partial \mathbf{B}/\partial t = 0$.

Since the beam length is much greater than the beam radius, and the beam's radial expansion takes place over a distance large compared to the beam length, the transverse electric field can be approximated to the lowest order by

$$E_r^{\text{inside}} = \frac{\rho(z) r}{2\varepsilon_0} \quad , \tag{A.3}$$

$$E_r^{\text{outside}} = \frac{\lambda}{2\pi\varepsilon_0 r} \quad , \tag{A.4}$$

where r is the radial coordinate.

Substituting Eq. A.3 into the azimuthal component of Eq. A.1, we obtain the longitudinal electric field

$$E_z(r,z) = E_z(0,z) + \frac{\rho'(z)}{4\varepsilon_0} r^2 \quad . \tag{A.5}$$

Substituting this expression into Eq. A.2 and integrating with respect to r, we obtain the transverse electric field to third order

$$E_r(r,z) = \frac{\rho r}{2\varepsilon_0} - E_z'(0,z)\frac{r}{2} - \frac{\rho''}{16\varepsilon_0} r^3 \quad . \tag{A.6}$$

The longitudinal electric field on axis $E_z(0,z)$ can be obtained if the electric potential Φ on axis is known. Integrating $E_r = -\partial\Phi/\partial r$ from $r = 0$ to $r = b$ and using Eqs. A.3 and A.4, the potential on axis is found to be

$$\Phi(0,z) = \frac{\lambda}{2\pi\varepsilon_0} \ln\left(\frac{b}{a}\right) = \frac{\rho z}{4\varepsilon_0} a^2 \quad .$$

Since the line charge density ρa^2 is a constant, we have

$$E_z(0,z) = \frac{\lambda}{2\pi\varepsilon_0 a} a' \quad . \tag{A.7}$$

The components for Eq. A.6 in the x and y directions can now be expressed as

$$E_x(x,z) = \left[\frac{\rho}{2\varepsilon_0} - \frac{\lambda a''}{4\pi\varepsilon_0 a} + \frac{\lambda}{4\pi\varepsilon_0}\left(\frac{a'}{a}\right)^2\right] x - \frac{\rho''(z)}{16\varepsilon_0} r^2 x \quad , \tag{A.8}$$

$$E_y(y,z) = \left[\frac{\rho}{2\varepsilon_0} - \frac{\lambda a''}{4\pi\varepsilon_0 a} + \frac{\lambda}{4\pi\varepsilon_0}\left(\frac{a'}{a}\right)^2\right] y - \frac{\rho''(z)}{16\varepsilon_0} r^2 y \quad . \tag{A.9}$$

Using these expressions, we can now derive the equation of motion to third order.

Since we are studying the beam in the expansion section in this Appendix, the external magnetic field is zero. Thus Eq.1 becomes

$$\frac{d}{dt} m\mathbf{v} = Ze\mathbf{E} \quad . \tag{A.10}$$

If we assume the particle mass is constant, then the x, y, and z components of this equation are

$$x''\dot{z}^2 + x'\ddot{z} = \frac{Ze}{m} E_x \quad , \tag{A.11}$$

$$y''\dot{z}^2 + y'\ddot{z} = \frac{Ze}{m} E_y \quad , \tag{A.12}$$

$$\ddot{z} = \frac{Ze}{m} E_z \quad . \tag{A.13}$$

Constancy in total energy T allows us to write velocity in the z direction as

$$\dot{z} = \sqrt{\frac{2T}{m}\left(1 - \frac{\varphi}{T} - \frac{\varepsilon_x}{T} - \frac{\varepsilon_y}{T}\right)} \quad , \tag{A.14}$$

where $\varphi = Ze\Phi, \varepsilon_x \equiv (m/2)\dot{x}^2$, and $\varepsilon_y \equiv (m/2)\dot{y}^2$.

Inserting Eqs. A.7 to A.9 and Eqs. A.13 and A.14 into Eqs. A.11 and A.12, the equations of motion to third order are

$$x'' + kx = \frac{Ze}{2T}\left\{\frac{\lambda a'}{2\pi\varepsilon_0 a}x' - \left[\frac{\lambda a''}{4\pi\varepsilon_0 a} - \frac{\lambda}{4\pi\varepsilon_0}\left(\frac{a'}{a}\right)^2 + \frac{\rho'' r^2}{16\varepsilon_0}\right]x\right\} \quad , \tag{A.15}$$

$$y'' + ky = \frac{Ze}{2T}\left\{\frac{\lambda a'}{2\pi\varepsilon_0 a}y' - \left[\frac{\lambda a''}{4\pi\varepsilon_0 a} - \frac{\lambda}{4\pi\varepsilon_0}\left(\frac{a'}{a}\right)^2 + \frac{\rho'' r^2}{16\varepsilon_0}\right]y\right\} \quad . \tag{A.16}$$

Terms inside the bracket on the right-hand-side of Eqs. A.15 and A.16 are of the same order of magnitude. These terms are at least an order of magnitude smaller than the electric field terms in Eq. 4. For example, the first term on the right-hand-side of Eq. A.15 and the electric field term on the right-hand side of Eq. 4 are about the same order of magnitude. Since we have demonstrated that the electric field terms in Eq. 4 are small compared with the magnetic field terms, the terms on the right-hand side of Eqs. A.15 and A.16 can be neglected.

APPENDIX B: OBTAINING OCTUPOLE STRENGTHS USING THE METHOD OF LEAST SQUARES WITH CONSTRAINTS

Once the positions of the six octupoles are determined, we allow the octupole strengths to be independent and find their strengths by minimizing the sum of the squares of their strengths. In others words, it is a least-squares problem with constraints. Least-squares solutions are normally used when there are fewer unknowns than conditions to be satisfied. Since all of the conditions cannot (in general) be satisfied exactly, one seeks the approximate solution that minimizes the sum of the squares of the residuals (the differences between the approximate and exact solutions).

The least-squares solution to a set of linear equations can be found as follows: Express the system of equations in matrix form as

$$\mathsf{A}\mathbf{x} = \mathbf{b} \quad , \tag{B.1}$$

where A is the coefficient matrix, $\mathbf{x}$ is the column vector of the unknowns and $\mathbf{b}$ is the column vector of the conditions to be satisfied. In the standard least-squares problem, there are more conditions than unknowns, so Eq. B.1 cannot be solved directly. However the least-squares solution is found by multiplying both sides of Eq. B.1 by the transpose of A,

$$\mathsf{A}^{\mathrm{T}}\mathsf{A}\mathbf{x} = \mathsf{A}^{\mathrm{T}}\mathbf{b} \quad , \tag{B.2}$$

and solving the resultant linear system for $\mathbf{x}$,

$$\mathbf{x} = [\mathsf{A}^{\mathrm{T}}\mathsf{A}]^{-1}\mathsf{A}^{\mathrm{T}}\mathbf{b} \quad . \tag{B.3}$$

Equation B.2 is the same linear system obtained when one forms the residual

$$R^2 = [\mathsf{A}\mathbf{x} - \mathbf{b}]^{\mathrm{T}}[\mathsf{A}\mathbf{x} - \mathbf{b}]$$

and minimizes R^2 by setting its partial derivative with respect to each x_i equal to zero.

In our situation, we wish to find a set of octupole strengths that cancel the aberrations produced by the quadrupole fringe fields. To prevent the required octupole strengths from being too large, we will use more octupoles than conditions to be satisfied, for example six octupoles to satisfy three conditions. The matrix equation is

$$\mathsf{A}\mathbf{s} = \mathbf{h} \quad , \tag{B.4}$$

where $\mathbf{s}$ is the column vector of the octupole strengths and $\mathbf{h}$ is the column vector of the aberration coefficients (the right-hand sides of Eq. 12). Because $\mathbf{s}$ has more elements than $\mathbf{h}$, there are an infinite number of solutions. We seek the solution that minimizes the sum of the squares of the octupole strengths. Equation B.4 is then augmented to be

$$\left[\frac{\mathsf{A}}{\mathsf{I}}\right]\mathbf{s} = \left[\frac{\mathbf{h}}{\mathbf{0}}\right] \quad , \tag{B.5}$$

where I is the identity matrix and $\mathbf{0}$ is a null vector. The left-hand side is further partitioned as

$$\left[\begin{array}{c|c} \mathsf{A}_1 & \mathsf{A}_2 \\ \hline \mathsf{I}_1 & \mathsf{I}_2 \end{array}\right]\left[\frac{\mathbf{s}_1}{\mathbf{s}_2}\right] = \left[\frac{\mathbf{h}}{\mathbf{0}}\right] \quad , \tag{B.6}$$

so that the upper partition can be used for finding the relation between $\mathbf{s}_1$ and $\mathbf{s}_2$ that exactly satisfies the aberration constraints $\mathbf{h}$:

$$\mathbf{s}_1 = \mathsf{A}_1^{-1}[\mathbf{h} - \mathsf{A}_2\mathbf{s}_2] \quad . \tag{B.7}$$

The lower partition gives

$$\mathsf{I}_1\mathbf{s}_1 + \mathsf{I}_2\mathbf{s}_2 = 0 \quad . \tag{B.8}$$

Substituting Eq. B.7 into Eq. B.8 and rearranging terms gives

$$[\mathsf{I}_2 - \mathsf{I}_1\mathsf{A}_1^{-1}\mathsf{A}_2]\mathbf{s}_2 = -\mathsf{I}_1\mathsf{A}_1^{-1}\mathbf{h} \quad . \tag{B.9}$$

The elements of $\mathbf{s}_2$ are found by solving Eq. B.9 in a least-squares sense as described above, and $\mathbf{s}_1$ is obtained from Eq. B.7.